Baghdad Science Journal

Volume 23 | Issue 1 Article 16

1-1-2026

Assessment of Carbon Capture Potential in Rubber Plantations via Landsat 9 Imagery Analysis

Ade Fitria
Department of Agrotechnology, Faculty of Agriculture, Universitas Sumatera Utara, Medan 20155, North Sumatra, Indonesia, fitriaa025@gmail.com

Rahmawaty Rahmawaty
Forestry Study Program, Faculty of Forestry, Universitas Sumatera Utara, North Sumatra, Indonesia AND Natural Resources and Environment Management Study Program, Postgraduate School, Universitas Sumatera Utara, Medan 20155, North Sumatra, Indonesia, rahmawaty@usu.ac.id

Razali Razali
Natural Resources and Environment Management Study Program, Postgraduate School, Universitas Sumatera Utara, Medan 20155, North Sumatra, Indonesia, razali@usu.ac.id

Jamin Saputra
Sungai Putih Research Unit, Deli Serdang 20585, North Sumatra, Indonesia, jamin.sbw@gmail.com

Seca Gandaseca
Faculty of Applied Sciences, Universiti Teknologi MARA (UiTM) Shah Alam, Selangor Darul Ehsan, Malaysia AND Institute for Biodiversity and Sustainable Development (IBSD), Universiti Teknologi MARA (UiTM) Shah Alam, Selangor Darul Ehsan, Malaysia, seca@uitm.edu.my

How to Cite this Article

Fitria, Ade; Rahmawaty, Rahmawaty; Razali, Razali; Saputra, Jamin; and Gandaseca, Seca (2026) "Assessment of Carbon Capture Potential in Rubber Plantations via Landsat 9 Imagery Analysis," *Baghdad Science Journal*: Vol. 23: Iss. 1, Article 16.
DOI: https://doi.org/10.21123/2411-7986.5145

BAGHDAD SCIENCE JOURNAL 2026;23(1):204–218

SPECIAL ISSUE ARTICLE

Assessment of Carbon Capture Potential in Rubber Plantations via Landsat 9 Imagery Analysis

Ade Fitria [1], **Rahmawaty** [2,3,*], **Razali** [3], **Jamin Saputra** [4], **Seca Gandaseca** [5,6]

[1] Department of Agrotechnology, Faculty of Agriculture, Universitas Sumatera Utara, Medan 20155, North Sumatra, Indonesia
[2] Forestry Study Program, Faculty of Forestry, Universitas Sumatera Utara, North Sumatra, Indonesia
[3] Natural Resources and Environment Management Study Program, Postgraduate School, Universitas Sumatera Utara, Medan 20155, North Sumatra, Indonesia
[4] Sungai Putih Research Unit, Deli Serdang 20585, North Sumatra, Indonesia
[5] Faculty of Applied Sciences, Universiti Teknologi MARA (UiTM) Shah Alam, Selangor Darul Ehsan, Malaysia
[6] Institute for Biodiversity and Sustainable Development (IBSD), Universiti Teknologi MARA (UiTM) Shah Alam, Selangor Darul Ehsan, Malaysia

ABSTRACT

Indonesia is a significant greenhouse gas (GHG) emitter, contributing 12.3% of carbon dioxide (CO_2) of total emissions. Carbon dioxide (CO_2), a major GHG, is increasing in the Earth's atmosphere. The CO_2 absorption can be increased through rubber plantations because rubber plants, such as forest plants, can process CO_2 as a carbon source for photosynthesis. This research aims to analyze carbon uptake in relation to tree density, biomass of rubber vegetation, and soil organic carbon (SOC) content, as well as to map the distribution of carbon potential using remote sensing. This research was conducted in the Sungai Putih Research Unit, Galang Sub-district, using a survey method by collecting secondary and primary data. Sampling locations were determined based on Normalized Difference Vegetation Index (NDVI) classification, while remote sensing image processing utilized Landsat 9 images processed through Google Earth Engine (GEE). This study found that the potential carbon stock varied across observation plots. Based on calculations using the SAVI Quadratic model (A13), carbon distribution, derived from field biomass (40–80) and C-Organic (2-3), indicated a medium carbon distribution. The average potential carbon stock, measured from the standing trunk section, was 29.43 tons across an area of 3.12 ha. The highest carbon stock and the largest average stem diameter were recorded in plot 11, with an average diameter of 16.63 cm and a biomass content of 90.64 kg.

Keywords: Agroforestry, GEE, *Hevea brasiliensis*, Machine learning, Vegetation index

Introduction

Estimating carbon sequestration in rubber plantations using Landsat 9 and Google Earth Engine (GEE) imagery has emerged as a promising approach to monitor and estimate the carbon storage capacity of this important agricultural system. Rubber plantations greatly influence global carbon dynamics, especially in Southeast Asia, which cultivates many rubber plant.[1,2] Indonesia has extensive rubber plantations compared to mangroves and acacias, and Indonesia is one of the main producers of greenhouse gases (GHG), contributing 2,31%[3] of global emissions. Therefore, to maintain the ecological function of forests as buffers for living systems in the face of declining forest areas, we need to improve their quality. The selection of rubber plants is based on their important ecological and economic roles. Ecologically,

Received 1 March 2025; revised 11 May 2025; accepted 20 May 2025.
Available online 1 January 2026

* Corresponding author.
E-mail addresses: fitriaa025@gmail.com (A. Fitria), rahmawaty@usu.ac.id (Rahmawaty), razali@usu.ac.id (Razali), jamin.sbw@gmail.com (J. Saputra), seca@uitm.edu.my (S. Gandaseca).

International Conference on Discoveries in Applied Sciences and Applied Technology (DASAT2025)
https://doi.org/10.21123/2411-7986.5145

rubber plantations serve as semi-natural ecosystems that can absorb carbon dioxide (CO_2) from the atmosphere. Economically, they provide the primary source of livelihood for millions of farmers. Additionally, rubber trees contribute to carbon absorption, helping to balance atmospheric CO_2 levels. The rise in CO_2 emissions must be counterbalanced by effective sequestration efforts. Landsat 9, introduced in September 2021, features higher spectral and radiometric resolution than previous generations, enabling more accurate detection of rubber plantations and biomass estimation.[4] Various studies have shown that vegetation indices such as NDVI, GNDVI, and SAVI are effectively used in remote sensing to combine health and density,[5–7] and vegetation changes in various ecosystems, including mangroves, rubber plantations, oil palms, and urban green spaces. NDVI is widely applied to assess vegetation density and health over time, such as in mangrove forests on Dompak Island,[5] rubber plantations, and land use changes in various regions.[5,8] GNDVI provides advantages in assessing biomass and vegetation health[9,10] in agricultural and forest environments and monitoring ecological risks in various ecoregions.[11,12] SAVI is used to reduce the influence of soil background in vegetation analysis12, is effective in distinguishing vegetation types,[13] and combines the impact of urbanization on green spaces.[14] Combining these vegetation indices with remote sensing technology and cloud computing platforms such as Google Earth Engine enables accurate and efficient vegetation dynamics and carbon stocks analysis in large areas.[14] When combined with the Google Earth Engine's cloud-based computing capabilities, SAVI enables efficient processing and analysis of large-scale satellite images to measure carbon stocks over very large areas.[15]

This method integrates spectral indices, texture analysis, and machine learning to estimate the above-ground biomass and carbon content in rubber plantations. Time series analysis enables monitoring variations of carbon sequestration variations over time, offering valuable insights into the impact of plantation expansion and management strategies on regional carbon budget.[16] Integrating remote sensing techniques with ground-based observations and allometric equations enables the development of credible models to predict carbon stocks in rubber plantations across different age classes and environmental conditions.[2,17] This GEE-based methodology[18] provides a cost-effective and scalable alternative for measuring carbon sequestration in rubber-dominated landscapes, supporting climate change mitigation and informing sustainable land management practices.[1] GEE is capable of producing spatial data and information on the earth's surface using multi-temporal satellites massively on satellite images quickly, over a wide area.[19] Spatial resolution is not sufficient for detecting individual details of rubber trees. Field validation requires extensive ground truthing to ensure high accuracy. The allometric model must be specific to rubber trees and properly validated. Additionally, vegetation variation, including the presence of weeds, shrubs, and the age of trees, makes it challenging to distinguish different factors. Atmospheric conditions such as clouds and fog can interfere with image quality. Lastly, the correlation between vegetation and carbon indices is not always profound.

This study aimed to characterize carbon stocks in rubber plantations using plot-based field measurements, soil samples, and remote sensing data to develop a simple remote sensing-based methodology. Field measurements and remote sensing approaches can improve rubber carbon stock estimation, aid emissions reduction efforts, and support program design incentives. Furthermore, this approach may improve rubber plantation management for climate change mitigation. The findings are expected to quantify carbon stock in rubber vegetation and assess its role and carbon emissions absorption. Studies on carbon stock estimation in rubber plantations can aid in assessing carbon emissions, contributing to climate regulation and global warming mitigation, analyzing carbon uptake in relation to tree density and rubber vegetation biomass, evaluating carbon content based on soil organic carbon, and mapping the potential distribution of carbon content using the selected estimation model.

Material and methods

Research location

This research was conducted at the latitude and the longitude of Sungai Putih Research Unit, which are roughly 3.4268803^0 N, 98.8681448^0 W, Galang, North Sumatra, located in Sungai Putih Village, Galang Sub-district, Deli Serdang Regency (see Fig. 1). This site is approximately 45 km south of Medan and 27 km from Lubuk Pakam, at an altitude of about 80 m above sea level. Access to the location includes an asphalt road from Medan to Sungai Putih, with the remaining route partially paved. The boundaries of the Sungai Putih Research Unit are as follows: the north borders Petumbukan Village and PT Perkebunan Nusantara III; the south is bordered by Perkebunan Tanjung Purba; the east is adjacent to Galang Sub-district and PTPN III; and the west borders the Bangun Purba area and PT. Serdang Tengah.

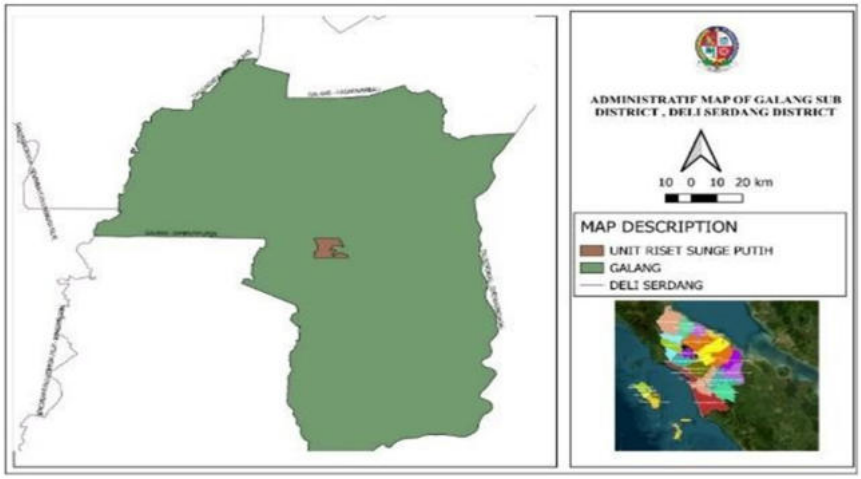

Fig. 1. Research location map.

Table 1. Tools and materials.

Tools	Information	Material
Hardware	computers/laptops	Administrative map
	GPS (Global Positioning System)	Sentinel 2
Software	QGIS (Quantum Geographic Information System)	Landsat 9
	GEE (Google Earth Engine)	SPOT
	compass	ASTER
Tools used in the laboratory	Analytical Balance	
	Volumetric flask 100 mL	Material use in the laboratory
	Erlenmeyer 500 ml	Sulfuric Acid (H_2SO_4)-concentrated
	Graduated pipette	Potassium Dichromate 1 N ($K_2Cr_2O_7$)
	Beaker Glass	Standard Solution 5.000 ppm C
	Burette	
Tools used in the field	Hoe	
	Soil drill	
	Plastic	
	Label paper	
	Twin pen	
	Rope	
	Meter	
	Whiteboard marker	
	notebook	

Tools and materials

Table 1. The tools and materials used for the research.

Research implementation method

This study uses a survey method consisting of several stages: primary and secondary data collection, selection of sample locations based on land availability, plant age, and soil type, determination of sample points using a homogeneous approach by assessing the health of rubber plants, because normal tree conditions affect plot locations, and soil analysis and remote sensing image processing. The collected data were analyzed using regression analysis to determine the relationship between satellite imagery and actual field data. We are making efforts to measure and map the potential for carbon absorption spatially in large area units (landscape-level), extending beyond just land units or small plots. This approach allows regional analysis using remote sensing data, such as Landsat 9 satellite imagery, to estimate the carbon content or stock stored in vegetation and soil in rubber plantation landscapes. With a medium scale (30 meters spatial resolution), Landsat 9 imagery is representative enough to describe variations in land cover and differences in vegetation conditions at the landscape level.

Table 2. NDVI classification class criteria.

Class	Classification Criteria
Barren land/water	NDVI > 0
Very low	0 < NDVI > 0,2
low	0,2 < NDVI > 0,4
Moderately low	0,4 < NDVI > 0,6
Moderately high	0,6 < NDVI > 0,8
high	0,8 < NDVI < 1

Determination of sample location points

The selection of coordinate points for field sampling is conducted using three methods:

1. Generating a map of the study area using Google Earth and QGIS[20,21]
2. Classifying the NDVI sampling area into five classes using the QGIS[22–25] application, and
3. Applying the NDVI classification criteria outlined in Table 2.

(1) The Avenza map application determines sampling locations for each class (coordinates) and different distances depending on the NDVI class taken. The results of these three steps are presented in Fig. 2, sampling coordinate points.

Sampling in the field

At this stage, primary data collection involves recording coordinate points. The sampling method used for collecting coordinate data and establishing[26] 25 m x 25 m sample plots follows a study-based approach with 50 plots. Soil sampling is conducted after making each plot with tape and recording it on the measurement form. A total of 50 soil samples are collected, representing the land, as they account for 5% of the total area (61.15 Ha) with a minimum sampling intensity of 1%. Of these 50 samples, 30 are used to develop mathematical models (training dataset), while the remaining 20 are used to assess model accuracy (test dataset).

Data analysis

Tree density and rubber trunk biomass

Field sampling utilizes GBH circumference data, which is converted to diameter at breast height (DBH) before applying a formula to obtain AGB.[27,28] The GBH is measured at a height of 1.5 m above ground level, approximately at an adult's chin level. The AGB of each tree in a plot is summed to determine the total AGB for the plot, which is then recorded in tabular form. Observations of density and biomass are calculated based on the vegetation, with plot determination based on Ardiyaningrum et al.[29]

Data analysis in Eq. (1) and Eq. (2)

$$\text{Density} = \text{number of individuals of one species} / (\text{sample area}) \quad (1)$$

$$\text{Relative density} = (\text{density of a species} \times 100\%) / (\text{density of all species}) \quad (2)$$

Biomass data from the research, including diameter, tree species, and the number of individual stands, were analyzed to determine the above-ground

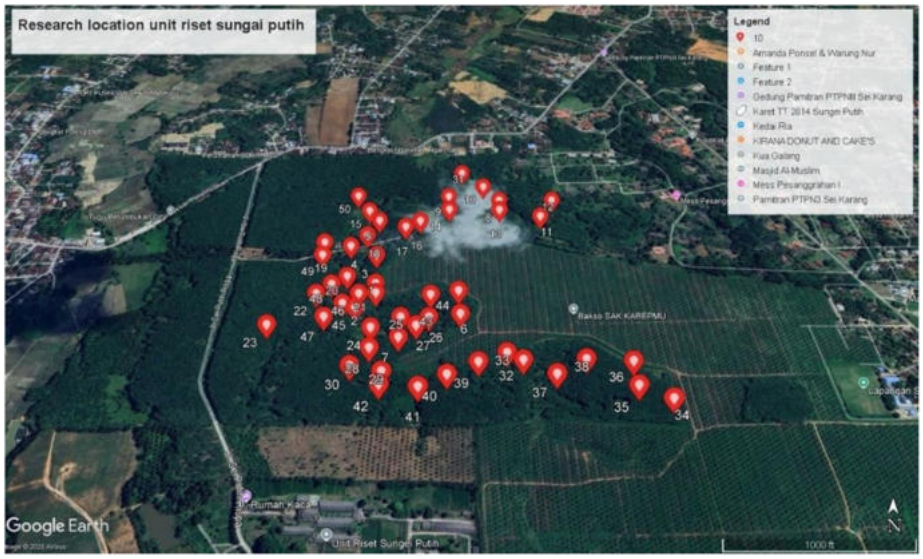

Fig. 2. Sampling coordinate points.

biomass of rubber trees and other plant species at the research site. The surface biomass of rubber trees was estimated using the allometric equation with the following formula in Eq. (3):

$$\text{AGBest} = -3.84 + (0.528 \text{ x BA}) + (0.001 \text{ x BA2}) \quad (3)$$

Description:

AGBEST: Above Ground Biomass value.
ρ: wood density (g/cm)
D: Diameter at breast height (cm) BA: basal area (cm)

The allometric equation proposed by Ketterings et al.[30] is used to estimate the value of above-ground biomass of non-rubber plants using the following formula in Eq. (4):

$$Y = 0.11\rho D.2.62 \quad (4)$$

Description:

Y: Above Ground Biomass value
ρ: wood density (g/cm)
D: Diameter at breast height (cm)

Biomass estimated using the selected model, along with biomass measurements obtained through the allometric equation referenced in Rahmawaty et al.,[31] is assumed to represent the actual biomass. Model validation in this study was conducted using the chi-square test, aggregate deviation (SA), and mean deviation (SR). The chi-square value was calculated using the following formula in Eq. (5):

$$xhitung^2 = \Sigma \text{ni} = (1(\hat{y} - y)2)/y \quad (5)$$

In addition, biomass measurement can be conducted using the allometric equation, as applied by Susilowati.[32] The equation is as follows in Eq. (6):

$$B = 0.11 \text{ x } \rho \text{ x } D2.62 \quad (6)$$

Description:

D = Diameter (cm)
ρ = Specific gravity of wood (g/cm^3)

Carbon estimation is conducted based on various variables in Landsat 9[33–36] magery, including digital values for each band as well as NDVI,[37–40] GNDVI,[9–11] and SAVI[12–15] indices. The model used for carbon estimation in Eqs. (7) to (10) is presented in Table 3.

Estimation results with actual biomass values. A lower aggregate deviation and mean deviation indicate higher model accuracy. The formulas for calculating SA and SR are as follows: The values of SA and SR can be calculated using the formulas provided in Eqs. (11) and (12):

$$SA = (\Sigma \hat{y}ni = 1 - \Sigma \hat{y}ni = 1)\Sigma \hat{y}ni = 1 \quad (11)$$

$$SR = \{|\Sigma \hat{y} - \Sigma \hat{y}ni = 1|n\} \quad (12)$$

Description:

SA = aggregate deviation
SR = average deviation
yy = actual biomass
$\hat{y}$ = estimated biomass
n = number of trees

Satellite imagery data was used to estimate carbon uptake based on digital NDVI,[37–40] GNDVI,[9–11] and SAVI[41] values from Landsat 9[42–45] for each subset observation plot. Table 4 shows the band characteristics of the Landsat 9 OLI satellite sensor, while Table 5 shows the vegetation indices used to estimate in Eqs. (13) to (15) carbon uptake in rubber vegetation.

Data classification and analysis based on Google earth engine

All the data processing for this study was conducted using cloud computing on the GEE platform, including land cover classification and spatial analysis. The first stage involved delineating the research area by cropping it based on shapefile data of the administrative boundaries of the Sunge Putih Research Center rubber plantation in the Galang sub-district, sourced from Google Earth in 2024.[46,47] The accuracy of image analysis results in the study area is significantly influenced by cloud cover. Therefore, image quality improvement was performed, particularly in cloud-covered areas, by applying a masking filter on the Quality Assessment (QA) band, which contains information on pixels affected by cloud cover. The masking script in GEE automatically replaces cloud-covered scenes with corrected ones within a predetermined recording time range. The scene selection process during masking is performed using the 'median ()' algorithm, where the GEE computing system selects the median value of each pixel from multiple scenes to minimize cloud cover, thereby generating a clearer image. The land cover classification results are then exported to the storage drive using the GEE script. This study used **QGIS**[48–50] to create a map layout of the land cover classification.

Table 3. Carbon estimation model.[48]

Model Type	Model	
Exponential Model	$Y = e^{(a+bX1+cX2+\cdots+nXn)}$	(7)
Quadratic Model	$Y = a + bX_1{}^2 + cX_2{}^2 + \ldots + nX_n{}^2$	(8)
Linear Model	$Y = a + bX_1 + cX_2 + \ldots + nX_n$	(9)
logarithmic model	$Y = a + bX_1{}^b + cX_2{}^c + \ldots + nX_n{}^n$	(10)

Table 4. Band characteristic of the landsat 9 OLI satellite sensor.

Band	Wavelength (μm)
Band 1 Visible Coastal Aerosol	0,43–0,45
Band 2 Blue	0,45–0,51
Band 3 Green	0,53–0,59
Band 4 Red	0,64–0,67
Band 5 Infrared Derat	0,85–0,88

a. Correlation regression test results

The normality test results were based on a correlation regression test on biomass, carbon uptake, and tree density. The analysis yielded p-values of 0.86 for biomass, 0.96 for carbon uptake, and 0.90 for tree density. Since all p-values exceed 0.05 ($p > 0.05$), the data are normally distributed, and the null hypothesis (H_0) is accepted. As shown in Figs. 3 to 5, the data points are distributed above and below zero on the Y-axis without forming a specific pattern, indicating the absence of heteroscedasticity.

b. Carbon estimation modelling

This study included a total of 50 observation plots, with 30 samples used for modelling. Table 6 presents the estimation model results based on these 30 samples.

Table 5. Vegetation indices used in estimating carbon sequestration in rubber vegetation.

Vegetation Index	Abbreviation	Formula	
Normalized Difference Vegetation Index	NDVI	$(NIR - Red)/(NIR + Red)$	(13)
Green Normalized Difference Vegetation Index	GNVI	$(NIR - Green)/(NIR + Green)$	(14)
Soil Adjusted Vegetation Index	SAVI	$(NIR - Red)/(NIR + Red + 0,16)$	(15)

Result and discussion

Carbon stock potential in a rubber plantation in the Galang sub-district

The potential carbon stocks obtained from each observation plot in this study varied. Aboveground carbon values were calculated for each tree within the observation plot. The average potential carbon stock in the field, based on the measurement of the standing trunk, was 29.43 tons/ha, with a total observed area of 3.12 ha. Field data analysis indicated that plot 11 had the highest carbon stock and the largest average stem diameter, measuring 16.63, with a biomass content of 90.64. The coordinates of this plot are 3043'05.75^0 N, 98086'6.686^0 W. According to research conducted by Anchopa and Lilian, 16-year-old rubber plants of clone PB 217 exhibit the largest stem diameter, measuring 94.92 cm. The carbon content in the biomass of rubber plants ranges from 45% to 50% of the dry matter. During a single planting cycle, rubber trees can absorb up to 97.65 tons of CO_2 per hectare, which includes 32.59 tons of CO_2 per hectare from litter and plant biomass. The determination of biomass is based on the stem diameter.[51] The spatial model of carbon content distribution in rubber is presented below.

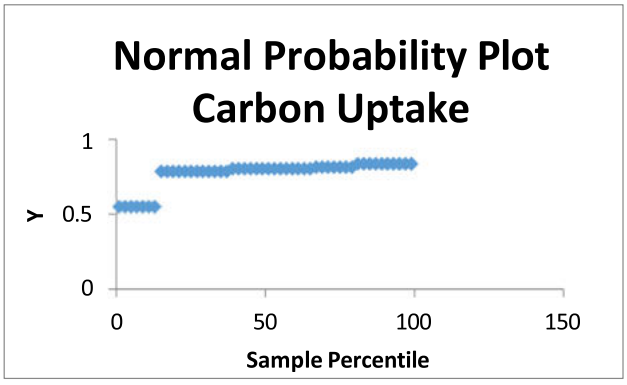

Fig. 3. Normality of carbon uptake.

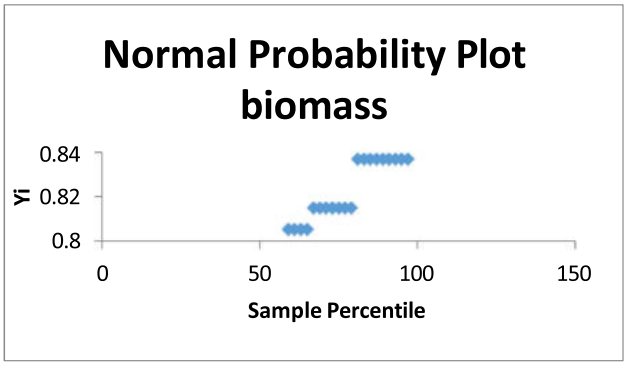

Fig. 4. Biomass normality.

Table 6. Regression equation model for carbon estimation based on vegetation.

Regression Model	Code	2021		2022		2023		2024	
		Sig Anova	R Square (R2)	Sig Anova	R Square (R2)	Sig Anova	R Square (R2)	Sig Anova	R Square (R2)
linier (NDVI)	A1	0.887	0.001	0.309	0.037	0.182	0.063	0.077	0.105
Logarithms (NDVI)	A2	0.899	0.001	0.127	0.081	0.004*	0.256	0.303	0.038
Quadratic (NDVI)	A3	0.072	0.117	0.241	0.1	0.009*	0.292	0.15	0.131
exponential (NDVI)	A4	0.873	0.001	0.209	0.056	0.214	0.055	0.079	0.106
linier (GNDVI)	A5	0.093	0.097	0.166	0.067	0.110	0.297	0.211	0.055
logarithms(GNDVI)	A6	0.020*	0.187	0.043*	0.139	0.009*	0.217	0.032*	0.154
Quadratic (GNDVI)	A7	0.011*	0.285	0.021*	0.249	0.001*	0.412	0.008*	0.303
exponential (GNDVI)	A8	0.104	0.092	0.185	0.062	0.120	0.084	0.230	0.051
linier (SAVI)	A9	0.057	0.357	0.013*	0.202	0.272	0.043	0.000*	0.361
logarithm(SAVI)	A10	0.055	0.125	0.000*	0.36	0.007*	0.231	0.010*	0.213
Quadratic (SAVI)	A11	0.000*	0.447	0.008*	0.304	0.000*	0.464	0.002*	0.374
exponential (SAVI)	A12	0.055	0.125	0.012*	0.205	0.308	0.037	0.000*	0.361

*Note * : significance at 5% error rate*

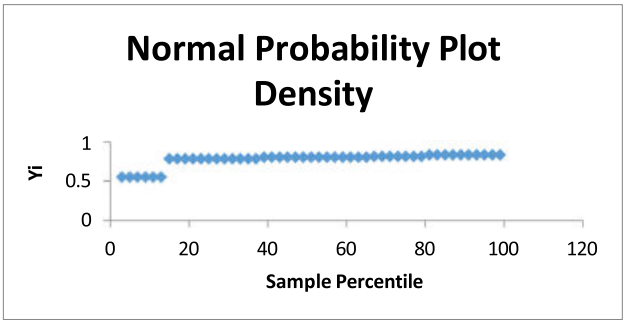

Fig. 5. Normality of tree density.

Based on Table 6, the ANOVA test results at a 5% significance level (sig ANOVA < 0.05) indicate that the following equation models are significant: in 2021 the NDVI logarithm, quadratic NDVI, and quadratic SAVI equation models; in 2022 the GNDVI logarithm, quadratic GNDVI, linear SAVI, logarithmic SAVI, quadratic SAVI, and exponential SAVI models; in 2023 the NDVI logarithm, quadratic NDVI, logarithmic GNDVI, quadratic GNDVI, logarithmic SAVI, and quadratic SAVI models; and in 2024 the logarithmic GNDVI, quadratic GNDVI, linear SAVI, logarithmic SAVI, quadratic SAVI, and exponential SAVI models. The R-Square (R2) values range from 0.001 to 0.447 in 2021, 0.037 to 0.304 in 2022, and 0.037 to 0.464 in 2023. In 2021, the quadratic model (SAVI) had the highest coefficient of determination (R2 = 0.447). In 2022, the quadratic model (SAVI) had an R^2 value of 0.367, followed by R^2 = 0.464 in 2023 and R^2 = 0.374 in 2024. This indicates that the quadratic model explains the influence of the independent variable (X), namely the vegetation index, on the dependent variable (Y), carbon, by 44.7% in 2021, 36.7% in 2022, 46.4% in 2023, and 37.4% in 2024. Among the regression models tested, the SAVI quadratic regression model exhibited the highest coefficient of determination: 0.447 in 2021, 0.367 in 2022, 0.464 in 2023, and 0.374 in 2024. According to Yang et al,[52] the coefficient of determination ranges from 0 to 1, where a value closer to 0 indicates a weaker effect.

Modelling is conducted to facilitate the development of regression models. This process aims to visualize the difference in vegetation index distribution within the image display, which serves as a reference for selecting an appropriate carbon estimation model. The distribution of the vegetation index distribution is presented in Figs. 6 to 8, as presented below:

c. Model validation test

The validation test for the regression equation model was conducted using 20 samples. The results of the validation test are presented in Table 7, as follows:

The regression equation models for the NDVI and GNDVI vegetation indices, as well as SAVI, passed the significance test in ANOVA, allowing all models to proceed to validation. The validation test assessed the deviation of carbon estimates from each regression model compared to the actual carbon values. The validation test aims to identify the best regression model among those developed. According to Legesse et al,[53] the purpose of validation is to assess the accuracy of estimated data against theoretical data to construct a model for estimating carbon potential in real-world conditions.

Table 7 shows that the highest R-squared (R2) values were observed in the 2021 exponential NDVI (R2 = 0.124), the 2022 exponential SAVI (R2 = 0.003), the 2023 exponential NDVI (R2 = 0.095), and the 2024 exponential SAVI (R2 = 0.002). The

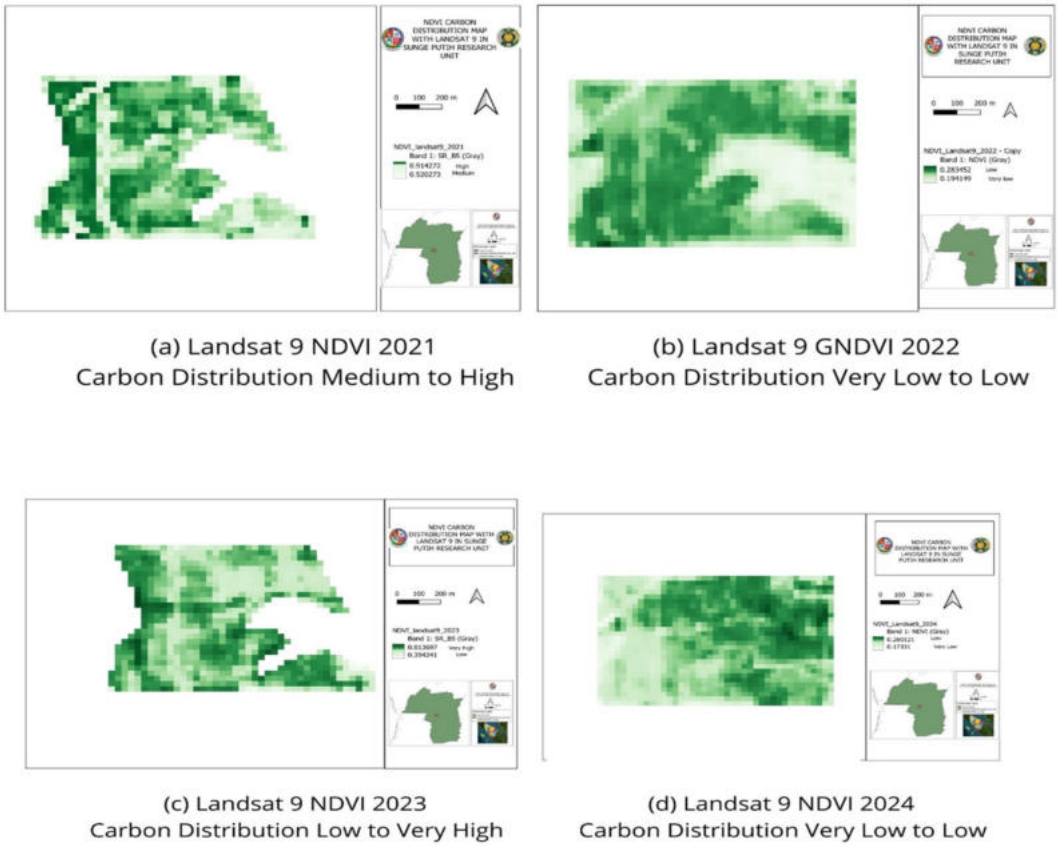

Fig. 6. Map of NDVI value distribution in rubber land areas.

selection of the model is based on both R2 and RMSE values.

d. Vegetation index distribution map on the selected regression model

The distribution map model selected based on R2 and RMSE values from 2021 to 2024 is predominantly represented by SAVI models. Therefore, the distribution map for the selected SAVI vegetation index is presented in Fig. 9 as follows:

The vegetation index distribution is based on the selected regression model that passed the validation test. The validation process included a paired-sample t-test to assess a significant difference between two related variables and a Root Mean Square Error (RMSE) test to measure the error rate in the regression model calculations. The vegetation index map from the selected model is used to assess how well it represents the actual vegetation conditions in the field. The distribution based on the selected model is shown in Fig. 6.

The Soil-adjusted Vegetation Index (SAVI) is an algorithm used to calculate or estimate vegetation index values from satellite images. This calculation utilizes bands 5 and 4 of the Landsat satellite. SAVI index values have demonstrated a strong and reliable correlation with biomass and carbon estimation, primarily due to their ability to minimize soil background interference in satellite images. This makes SAVI a suitable choice for biomass estimation across various land cover conditions. Fig. 4 illustrates the distribution of vegetation indices in rubber plantations, with index values ranging from 0.1 to 0.4. Within this range, variations in vegetation index values are observed. As shown in Fig. 9, the dominant vegetation index values range from 0.2 to 0.4, indicating relatively high vegetation canopy density. This aligns with the findings of Candra and Arsana,[54] who stated that dense vegetation cover corresponds to a high SAVI index value, while sparse vegetation cover results in lower values. The SAVI value reflects the presence of vegetation on the Earth's surface and serves to describe plantation conditions. A higher vegetation index value indicates greater vegetation density or land cover with green vegetation.

e. Map of carbon potential distribution using the selected estimation model

The selected model in this research is a quadratic model. Based on the determination of values in 2021,

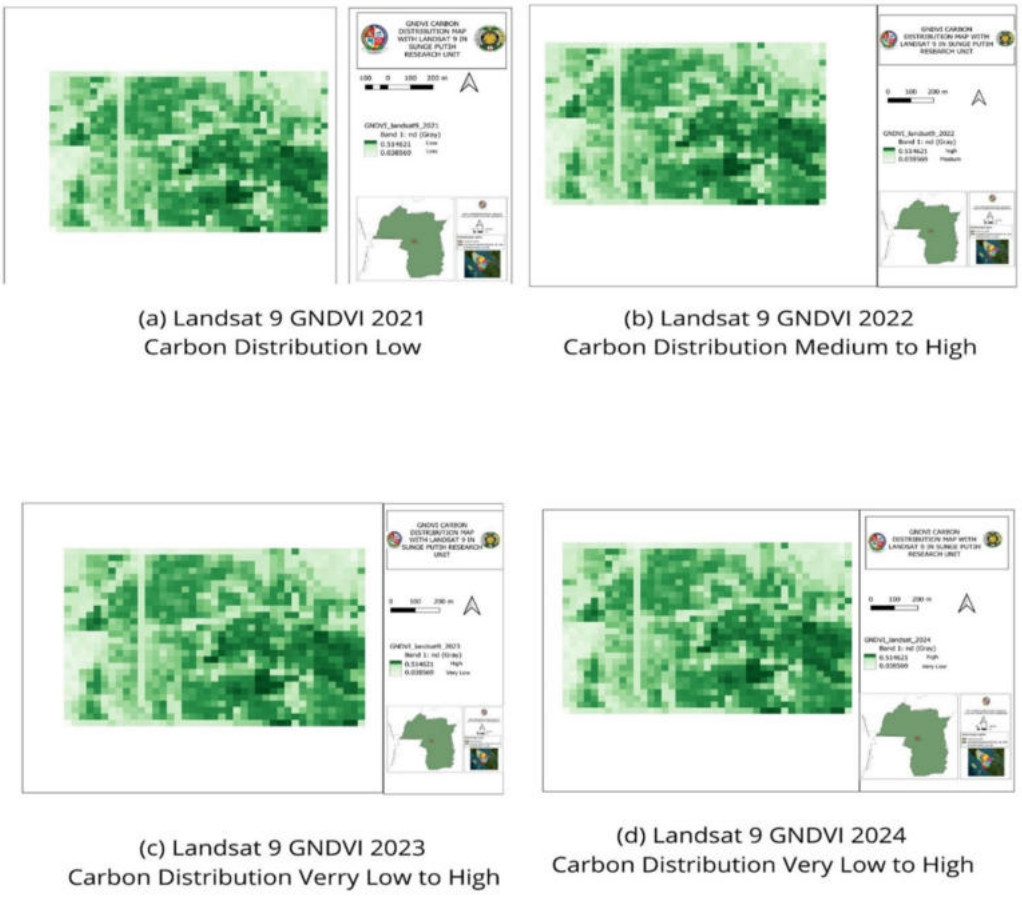

Fig. 7. Map of GNDVI value distribution in rubber land areas.

the highest R2 value for the quadratic SAVI model is 0.447, the lowest RMSE value is 0.000, and the significance level (p-value) for biomass and C-organic (two-tailed) is 0.000. In the 2022 quadratic Savi model, the highest R2 value is 0.304, the lowest RMSE value is 0.000, and the significance level (p-value) for biomass and C-organic (two-tailed) is 0.000. In the 2023 quadratic SAVI model, the highest R2 value is 0.464, the lowest RMSE value is 0.000, and the significance level (p-value) for biomass and C-organic (two-tailed) is 0.000. In the 2024 quadratic SAVI model, the highest R2 value is 0.374, the lowest RMSE value is 0.000, and the significance level (p-value) for biomass and C-organic (two-tailed) is 0.000. Therefore, the null hypothesis H0 is rejected, indicating a significant difference between the estimated and actual carbon values. This model will be used to analyze carbon distribution at the research site using the following in Eq. (16):

$$Y = -2.733E - 5 + 0.81 \times 2 \quad (16)$$

Based on calculations using the selected quadratic SAVI model (A3), the carbon distribution derived from field data ranges from 0.003 to 40 in areas with low carbon distribution and from 41 to 82 in areas with moderate carbon distribution. According to soil C-organic values, carbon distribution is classified as follows: 0.00002 to1 indicates very low distribution, 1 to 2 indicates low distribution, and 2 to 3 indicates medium distribution.

The carbon content in a tree is influenced by its biomass, as a higher biomass in a rubber tree corresponds to a greater carbon value. This aligns with the statement by Sulistiyono and Hudjimartsu,[32] which suggests that biomass content in trees, soil fertility, and vegetation uptake impact carbon storage. Additionally, higher biomass in vegetation is directly related to increased carbon content. Thus, an increase in the biomass of rubber vegetation corresponds to greater carbon storage within the vegetation. One of the factors influencing biomass value is age, as plant age is directly proportional to the diameter of rubber trees. Carbon storage in rubber plants is determined by various factors, including tree age, stem diameter, plant height and density, soil fertility, and the cultivation system used. Forest biomass components consist of aboveground biomass (AGB), belowground

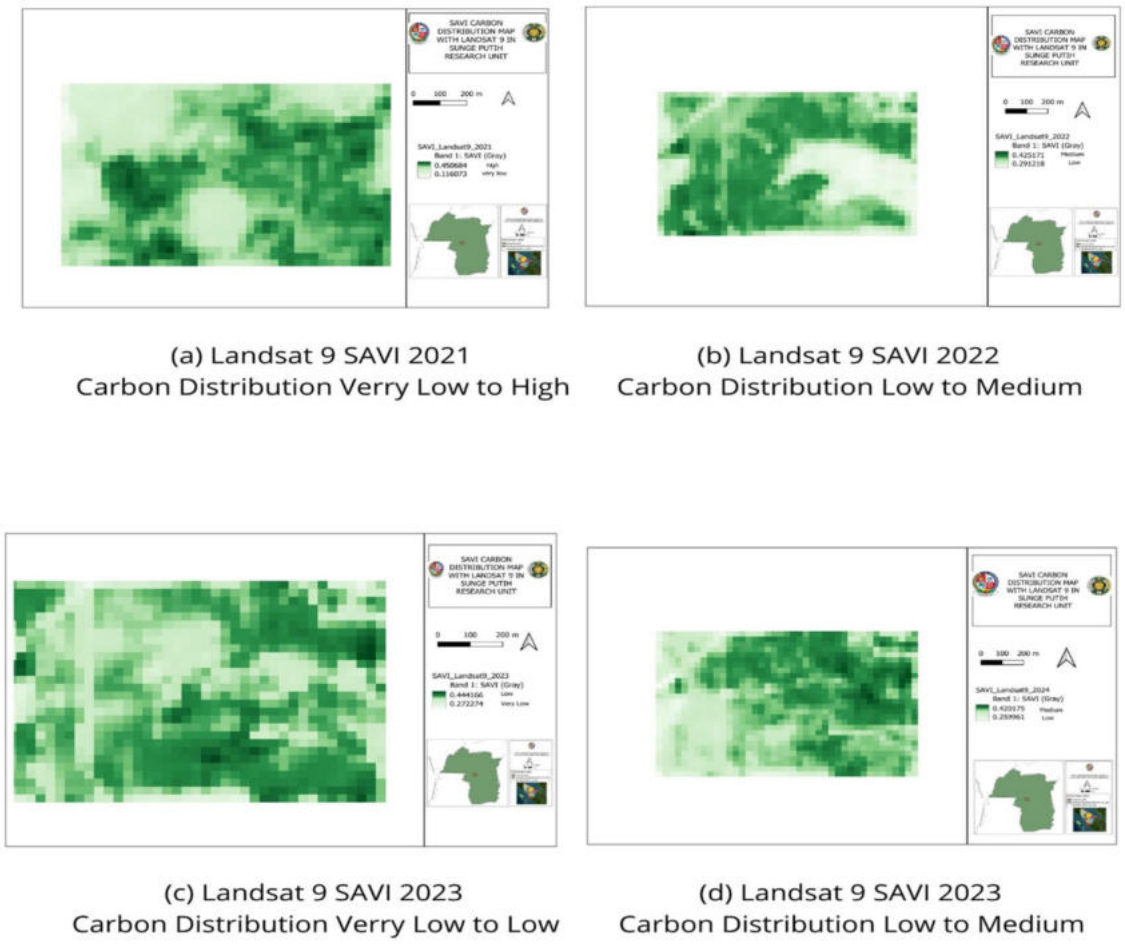

Fig. 8. Map of SAVI value distribution in rubber land areas.

Table 7. Validation test result.

		2021		2022		2023		2024	
Regression Model	Code	Sig T	RMSE	Sig T	RMSE	Sig T	RMSE	Sig T	RMSE
linear (NDVI)	A1	0,000	0.031	0.586	0,000	0,000	0.019	0.345	0,000
logarithm(NDVI)	A2	0,000	0.055	0.875	0,000	0.001	0.031	0.276	0,000
Quadratic (NDVI)	A3	0,000	0.020	0.373	0,000	0,000	0.013	0.525	0,000
exponential (NDVI)	A5	0,000	0.124	0.626	0.001	0,000	0.095	0.346	0.001
linear (GNDVI)	A6	0.221	0,000	0.365	0,000	0.429	0,000	0.22	0,000
logarithm(GNDVI)	A7	0.067	0,000	0.137	0,000	0.098	0,000	0.054	0,000
Quadratic (GNDVI)	A8	0.346	0,000	0.523	0,000	0.309	0,000	0.24	0,000
exponential (GNDVI)	A10	0.213	0.001	0.341	0.002	0.408	0.002	0.212	0.001
linear (SAVI)	A11	0.057	0.001	0.182	0.000	0,000	0,000	0.001	0,000
logarithm(SAVI)	A12	0.143	0.001	0.624	0.000	0.002	0,000	0.007	0,000
Quadratic (SAVI)	A13	0.124	0.001	0.03	0.000	0,000	0,000	0.004	0,000
exponential (SAVI)	A15	0.061	0.005	0.169	0.003	0,000	0.003	0.001	0.002

biomass (BGB), dead organic matter, and soil organic carbon.[55] Aboveground biomass comprises trees and plants, including trunks, branches, bark, and leaves that grow above the ground. The stage of a tree's development influences biomass distribution in an area, as reflected in variations in biomass across different tree diameters. Compared to belowground biomass, aboveground biomass contributes the most to total biomass and has a broader distribution. The contribution of biomass from each tree component varies significantly.[56] Time series analysis enables tracking variations in carbon sequestration over time, offering valuable insights into the impact of rubber plantation expansion and management strategies on regional carbon budgets.[17]

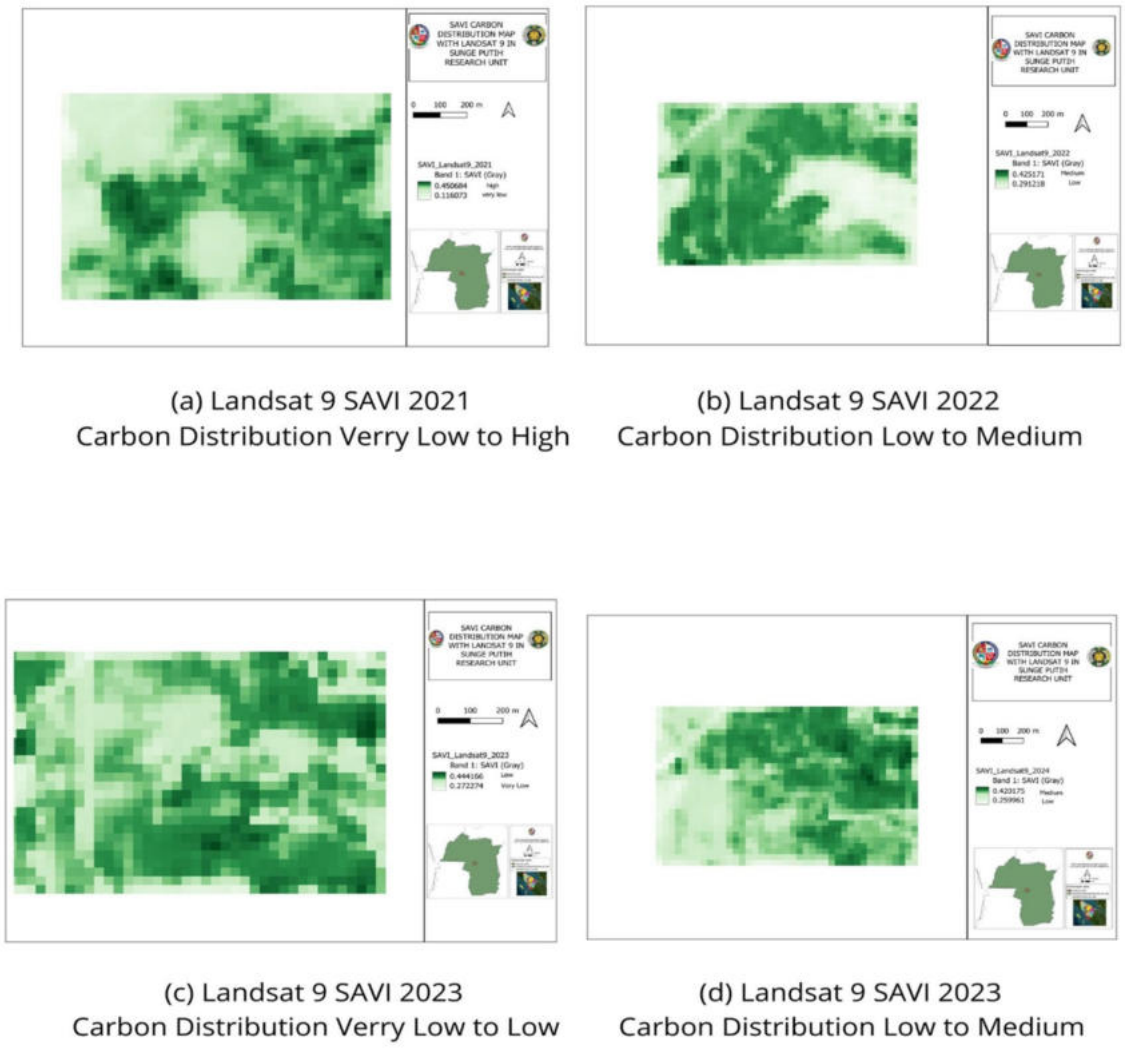

Fig. 9. Map of SAVI value distribution in rubber land areas.

Conclusion

The highest carbon reserves and the largest average stem diameter are found in plot 11, with an average diameter of 16.63 cm and a biomass content of 90.64 kg/ha. The best model, the quadratic SAVI model, has the highest coefficient of determination (R-square) values: R2 = 0.447 in 2021, R2 = 0.303 in 2022, R2 = 0.464 in 2023, and R2 = 0.374 in 2024. The carbon distribution is determined based on calculations using the selected SAVI (A13) quadratic model.

Acknowledgement

The author expresses gratitude to the Directorate of Research, Technology, and Community Service, which operates under the Directorate General of Higher Education, Research, and Technology in the Republic of Indonesia.

Authors' declaration

- Conflicts of Interest: None.
- We hereby confirm that all the Figures and tables in the manuscript are our original work. Furthermore, any figures and images that are not our own have been included with the necessary permission for republication, which is attached to the manuscript.
- No animal studies are present in the manuscript.
- No human studies are present in the manuscript.
- Ethical Clearance: The project was approved by the local ethical committee at Universitas Sumatera Utara, Medan 20155, North Sumatra, Indonesia.

Authors' contribution statement

A. F. and R. designed and conducted the experiments, collected field samples, analyzed and interpreted the data, and drafted the original manuscript. J.S., R., and S.G. contributed to data analysis and interpretation, as well as the review and editing of the manuscript.

Funding statement

Funding from the Directorate of Research, Technology, and Community Service under the Directorate General of Higher Education, Research, and Technology, Republic of Indonesia, for funding this study under scheme number 128/UN5.4.10.S/PPM/KP-DRTPM/2024.

References

1. Yunxia W, Peter M, Hollingsworth, Deli Z, Christopher D, West JMH, *et al.* High-resolution maps show that rubber causes substantial deforestation. Nat. 2023;623. https://doi.org/10.1038/s41586-023-06642-z.
2. Wei GL, Jia QZ, Yan Y, Philip BA, Christoph K, Gbadamassi GO, *et al.* Encouraging the reconversion of rubber plantations by developing a combined payment system. Glob Ecol Conserv. 2023;43. https://doi.org/10.1016/j.gecco.2023.e02415.
3. JRC Science for Policy Report. GHG Emissions All World Countries. European. 2023.
4. Rawee C, Buncha S, Sirima W, Apichet T, Supet JI. Investigating drivers impacting carbon stock and carbon offset in a large-scale rubber plantation in the middle South of Thailand. Trop Life Sci Res. 2024;35(1):139–160, https://doi.org/10.21315/tlsr2024.35.1.8.
5. Sabriyati D, Azzahra M, Andi Z. Mangrove density mapping from Landsat 8/9 OLI imagery in Dompak Island, Indonesia: A study from 2017 to 2022. BIO Web of Conf. 2023;70. https://doi.org/10.1051/bioconf/20237001010.
6. Taufan A, Lukman H, Taufiq WH, Era IP, Bejo A, Sri A. Analysis of differences in vegetation development in 2009 and 2022 in Semboro Sub-District, Jember Regency. Indonesian J Remote Sens Appl. 2023;1(01):42–48.
7. Wirawan STC, Chernovita HP. Analysis of vegetation changes using satellite imagery and normalized difference vegetation index (NDVI): A case study in Tuntang District, Semarang District. J Inf Syst Inform. 2023;5(4). https://doi.org/10.51519/journalisi.v5i4.622.
8. Khunrattanasiri W, Alongkorn A, Rianthakool L, Hutayanon T. Comparative study of Landsat 9 and Sentinel-2 satellite data for above-ground carbon sequestration estimation amae moh mine reforestation site, Lampang Province, Thailand. Agric Nat Resour. 2023;58:175–185. https://doi.org/10.34044/j.anres.2024.58.2.02.
9. Salinas VMG, Hectoe FM, Carlos AO. Evaluation of nitrogen status in a wheat crop using unmanned aerial vehicle images. Chil J Agric Res. 2021;81(3):408–419. https://doi.org/10.4067/S0718-58392021000300408.
10. Saleh MB, I Nengah SJ, Nitya AS, Dewayany S, Ita C, Zhang Y, Wang X, Liu Q. Algorithm for detecting deforestation and forest degradation using vegetation indices. TELKOMNIKA. 2019;17(5):2335–2345. https://doi.org/10.12928/telkomnika.v17i5.12585.
11. Liu Z, Jianhua S, Bing J, Xiaohui H, Dongmeng z, Chunlin W, *et al.* The dominant influencing factors of desertification and ecological risk changes in Qinghai area of qilian mountains national park: Climate change or human activity?. J Environ Manage. 2024:362. https://doi.org/10.1016/j.jenvman.2024.121335.
12. Jaraye AN, Helmi ZMS, Yuhao A, Yang PL, Shahrul AB, Haryati A, *et al.* Oil palm age estimation using broad-band and narrow-band vegetation indices derived from Sentinel-2 data. Asia-Pac J Sci Technol. 2023:29. https://doi.org/10.14456/apst.2024.30
13. Almutairi B, Ali EB, Mohamed AB, Nadir AHM. Comparative study of SAVI and NDVI vegetation indices in Sulaibiya Area (Kuwait) using worldview satellite imagery. Int J Geosci Geomatics. 2013:2052–5591.
14. Pattanakiat S, Sirasit V, Thamarat P, Pisut N, Theerawut C, Voravart RNB, *et al.* Spasial green space assessment in Suburbia: Implications for urban development. MDPI. Environ Nat Resour J. 2024;22(1):76–92. https://doi.org/10.32526/ennrj/22/20230153.
15. Agustiyara A, Dyah M, Achmad N, Aulia NK, Ikhwali MF. Mapping urban green spaces in indonesian cities using remote sensing analysis. MDPI. Urban Sci. 2025;9(2):23. https://doi.org/10.3390/urbansci9020023.
16. Fu Y, Hongjian T, Weili K, Weiheng X, Huan W, Ning L. Estimation of rubber plantation biomass based on variable optimization from Sentinel-2 remote sensing imagery. MDPI. Forest. 2024;15(6)900. https://doi.org/10.3390/f15060900.
17. Huang C, Chenchen Z, He L. Assessment of the impact of rubber plantation expansion on regional carbon storage based on time series remote sensingand the InVEST model. MDPI. Remote Sens. 2022;14(24):6234. https://doi.org/10.3390/rs14246234
18. Venkatappa M, Nophea S, Sutee A, Benjamin S. Applications of the Google Earth Engine and phenology-based threshold classification method for mapping forest cover and carbon stock changes in Siem Reap Province, Cambodia. MDPI. Remote Sens. 2022;12(18):3110. https://doi.org/10.3390/rs12183110.
19. Putri RA. and Rifka S. Land cover analysis using Google Earth Engine and Landsat 8 OLI imagery. J.Penelit. Ilmu Teknol. Komput. 2023:15(2):1031–1042. https://doi.org/10.5281/zenodo.10070659.
20. Adhikari G, Khagendra PJ, Dristee C, Ashish G, Sandeep M. Spatial Dynamics and Risk Mapping of Forest Fires in Madhesh Province, Nepal: A Multi-Criteria Decision Approach. MDPI. Environ Nat Resour J. 2025;23(1):80–94. https://doi.org/10.32526/ennrj/23/20240124.
21. Khalaf AB. Using remote sensing and geographic information system to study the change detection in temperature and Surface Area of Hamrin Lake. Baghdad Sci J. 2022;19(5):1130–1139. http://dx.doi.org/10.21123/bsj.2022.19.4.6420.
22. Samphutthanont R, Worawit S, Phathranit K, Kitisak P. Carbon sequestration assessment using satellite data and GIS at Chiang Mai Rajabhat University. MDPI. Environ Nat Resour J. 2024;22(6):574–584. https://doi.org/10.32526/ennrj/22/20240183.
23. Rahmawaty R, Frastika S, Rauf A, Batubara R, Harahap FS. Land suitability assessment for *Lansium domesticum* cultivation on agroforestry land using matching method and geographic

information system. Biodiversitas. 2020;21(8). https://doi.org/10.13057/biodiv/d210835.
24. Rahmawaty R, Samosir JB, Batubara R, Rauf A. Diversity and distribution of medicinal plants in the Universitas Sumatera Utara Arboretum of Deli Serdang, North Sumatra, Indonesia. Biodiversitas 2019;20(5). https://doi.org/10.13057/biodiv/d200539.
25. Rahmawaty, PP, Latifah S. Spatial analysis on distribution of green belt to reduce impacts of climate change in Medan City, North Sumatra. Malays Appl Biol. 2017;46(2):67–76.
26. Fararoda R, Reddy RS, Rajashekar G, Thangavelu M, Praveen M, Satish KV, *et al.* Improving plot- level above ground biomass estimation in tropical Indian Forests. MDPI. Ecol Informat. 2024:81. https://doi.org/10.1016/j.ecoinf.2024.102621.
27. Saputra J, Kamal M, Wicaksono P. Effect of image spatial resolution on mapping results of nitrogen nutrient content of rubber plantations. J Rubber Res. 2018;36(1):13–24. https://doi.org/10.22302/ppk.jpk.v36i1.545.
28. Maung WS, Satoshi T, Takuya H, San SH. Assessing above ground biomass of wunbaik mangrove forest in myanmar using machine learning and remote sensing data. MDPI. Disc Conserv 2025:2(8). https://doi.org/10.1007/s44353-025-00025-3
29. Aningrum ID, Maria TSB, Komariah. Short Communication: Species composition and diversity of vegetation in dry-land agricultural landscape. Biodiversitas. 2021:22(1):65–71. https://doi.org/10.13057/biodiv/d220109.
30. Ketterings QM, Choe R, Van-Noordwijk M, Ambagau Y, Palm CA. Reducing uncertainty in the use of allometric biomass equations for predicting above-ground tree biomass in mixed secondary forest. For Ecol Manag. 2001;146(1-3):199–209. https://doi.org/10.1016/S0378-1127(00)00460-6.
31. Dossa KF, Yan EM. Remote sensing methods and GIS approaches for carbon sequestration measurement: A general review. Int J Environ Clim Chang. 2024;14(7):222–233. https://doi.org/10.9734/ijecc/2024/v14i74265.
32. Sulistiyono N, Hudjimartsu SA. Potential of above-ground biomass (AGB) of mangrove vegetation restoration in Lubuk Kertang. IOP Conf Ser. Earth Environ Sci. 2021;782(3). https://doi.org/10.1088/1755-1315/782/3/032036.
33. Sun Y, Binyu W, Senlin T, Bingxin L, Zhouxu Z, Ying L. Continuity of top-of-atmosphere, surface, and nadir BRDF-adjusted reflectance and NDVI between Landsat-8 and Landsat-9 OLI over China landscape. MDPI. Remote Sens. 2023;15:4948. https://doi.org/10.3390/rs15204948.
34. Prasetyo AR, Niechi V, Hasyyati S. Landsat 9 imagery based mangrove forest mapping using maximum likelihood classifier and support vector machine algorithm. Agroteksos. 2023;33(3); 803–813 https://doi.org/10.29303/agroteksos.v33i3.975.
35. Mann J, Emily M, Mahesh S, Jeffrey I, Jeffrey CM, Aaron G, *et al.* Landsat 8 and 9 underfly international surface reflectance validation collaboration. MDPI Remote Sens. 2024;16(9):1492. https://doi.org/10.3390/rs16091492.
36. Jiang F, Hua S, Erxue C, Tianhong W, Yaling C, Qingwang L. Above-ground biomass estimation for coniferous forests in Northern China using regression kriging and Landsat 9 images. MDPI. Remote Sens. 2022;14(22):5734. https://doi.org/10.3390/rs14225734.
37. Agung S, Noverita DT, Raldi HK, Evi F. Diversity, biomass, covers, and NDVI of restored mangrove forests in karawang and subang coasts, West Java, Indonesia. Biodiversitas. 2021;22(9):4115–4122. https://doi.org/10.13057/biodiv/d220960.
38. Spadoni GL, Allicd CLC, Michele M. Analysis of normalized difference vegetation index (NDVI) multi-temporal series for the production of forest cartography. Remote Sens App Soci Environ. 2020;20:100419. https://dx.doi.org/10.1016/j.rsase.2020.100419.
39. Tigabu A, Agenagnew AG. Mapping forest cover change and estimating carbon stock using satellite derived vegetation indices in Alemsaga Forest, Ethiopia. Plos One. 2025;20(2):e0310780. https://doi.org/10.1371/journal.pone.0310780
40. Genç ÇÖ, Arif OA. Monitoring the operational changes in surface reflectance after logging, based on popular indices over Sentinel-2, Landsat-8, and ASTER imageries. Environ Monit Assess. 2025;197:120. https://doi.org/10.1007/s10661-024-13526-w.
41. Achmad E, Nursanti, Manalu JHB. Spatial model of above-ground biomass estimation in nagari padang Limau Sundai Forest, South Solok Regency, West Sumatra Province. J Silva Trop. 2018;2(3):67–76.
42. Anees SA, Kaleem M, Waseem RK, Muhammad S, Tahani AA, Sulaiman AA, *et al.* Integration of machine learning and remote sensing for above ground biomass estimation through Landsat-9 and field data in temperate forests of the Himalayan Region. Ecol Inform. 2024;82:102732. https://doi.org/10.1016/j.ecoinf.2024.102732.
43. Geng J, Qiuyuan T, Junwei L, Huajun F. Assessing spatial variations in soil organic carbon and C:N ratio in Northeast China's black soil region: Insights from Landsat-9 satellite and crop growth information. Soil Tillage Res. 2024;235:105897. https://doi.org/10.1016/j.still.2023.105897
44. Ahmad B, Mohammad BN, Shamshad A. Analysis of LST, NDVI, and UHI Patterns for urban climate using Landsat-9 Satellite data in Delhi. J Atmos Sol-Terr Phys. 2024;265:106359. https://doi.org/10.1016/j.jastp.2024.106359
45. Zhang Q, Difeng W, Dongyang F, Fang G, Xiangiang H, Yiqi W. Characterization of Landsat-8 and Landsat-9 Reflectivity and NDVI continuity based on Google Earth Engine. IEEE. J Sel Top Appl Earth Obs Remote Sens. 2025;18. https://doi.org/10.1109/JSTARS.2024.3492025.
46. Lemenkova P, Olivier D. Satellite image processing by python and R using Landsat 9 OLI/TIRS and SRTM DEM data on Côte d'Ivoire, West Africa. J Imaging. 2022;8(12):317. https://doi.org/10.3390/jimaging8120317.
47. Rahmawaty, Siahaan J, Nuryawan A, Harahap MM, Ismail MH, Rauf A, *et al.* Mangrove cover change (2005–2019) in the Northern of Medan City, North Sumatra, Indonesia. Geocarto Int. 2023;38(1):2228742. https://doi.org/10.1080/10106049.2023.2228742.
48. Belloli TF, Diniz CDA, Laurindo AG, Christhian SC, Carina CK. Modeling wetland biomass and aboveground carbon: influence of plot size and data treatment using remote sensing and random forest. MDPI. Land. 2025;14(3):616. https://doi.org/10.3390/land14030616.
49. Czimber K, Botond S, Nortbert A, David H, Gabor L, Diana M, *et al.* Estimation of the total carbon stock of dudles forest based on satellite imagery, airborne laser scanning, and field surveys. MDPI. Forest. 2025;16(3):512. https://doi.org/10.3390/f16030512
50. Rahmawaty R, Rauf A, Harahap MM, Kurniwan H. Land Cover change impact analysis: an integration of remote sensing, gis and dpsir framework to deal with degraded land in lepan watershed, North Sumatra, Indonesia. Biodiversitas. 2022;23(6). https://doi.org/10.13057/biodiv/d230627.

51. Anchoph Y, Lilian S. Availability of biomass in various clones of rubber (hevea brasiliensis) in dry land. JPT. 2023:11(2):95–102. https://doi.org/10.36084/jpt..v0i2.488.
52. Yang K, Kai L, Bo Q, Feiping W, Qinglin X, Jun C, *et al.* Estimating forest aboveground carbon sink based on landsat time series and its response to climate change. Sci Rep. 2025;15:589. https://doi.org/10.1038/s41598-024-84258-7.
53. Legesse F, Sileshi D, Teshome S. Estimating carbon stock using vegetation indices and empirical data in the upper awash river basin. Discov Environ. 2024;2:137. https://doi.org/10.1007/s44274-024-00165-8
54. Chandra SP, Arsana GNK. Land cover analysis using the soil adjusted vegetation index (SAVI) method. J Sains Riset. 2024;14(1):24-34. https://dx.doi.org/10.47647/jsr.v14i1.2095
55. Razaq M, Qicheng H, Feijun W, Changan L, Palingamoorthy G, Chenggang L, *et al.* Carbon stock dynamics in rubber plantations along an elevational gradient in tropical China. MDPI. Forests. 2024;15(11):1933. https://doi.org/10.3390/f15111933.
56. Zhang X, Yongzhi Z, Yuhui J, Mengyao Y, Xinyi L, Jie D, *et al.* Climate factors affect above belowground biomass allocation in broad-leaved and coniferous forests by regulating soil nutrients. MDPI. Plant. 2023;12(23):3926. https://doi.org/10.3390/plants12233926.

تقدير احتجاز الكربون في نباتات المطاط باستخدام القمر الصناعي لاندسات 9

أدي فيتريا[1]، رحمواتي[2،3]، رزالي[3]، جامين سابوترا[4]، سيكا غانداسيكا[5،6]

[1]قسم التكنولوجيا الزراعية، كلية الزراعة، جامعة سومطرة أوتارا، ميدان 20155، شمال سومطرة، إندونيسيا.
[2]برنامج دراسة الغابات، كلية الغابات، جامعة سومطرة أوتارا، شمال سومطرة، إندونيسيا.
[3]برنامج دراسة إدارة الموارد الطبيعية والبيئة، كلية الدراسات العليا، جامعة سومطرة أوتارا، ميدان 20155، شمال سومطرة، إندونيسيا.
[4]وحدة أبحاث سونغاي بوتيه، ديلي سيردانغ 20585، شمال سومطرة، إندونيسيا.
[5]كلية العلوم التطبيقية، جامعة التكنولوجيا مارا (*UiTM*) شاه علم، سيلانجور دار الاحسان، ماليزيا.
[6]معهد التنوع البيولوجي والتنمية المستدامة (*IBSD*)، الجامعة التكنولوجيا.
مارا (*UiTM*) شاه علم، سيلانجور دار الإحسان، ماليزيا.

الملخص

إندونيسيا هي من بين أكبر مصادر غازات الاحتباس الحراري، حيث تسهم بنسبة 12.3% من انبعاثات ثاني أكسيد الكربون الإجمالية. يعتبر ثاني أكسيد الكربون(CO2) ، وهو من الغازات الدفيئة الرئيسية، في ازدياد في الغلاف الجوي للأرض. يمكن زيادة امتصاص CO_2من خلال مزارع المطاط لأن نباتات المطاط، مثل نباتات الغابات، تستطيع معالجة CO_2 كمصدر للكربون في التمثيل الضوئي. يهدف هذا البحث إلى تحليل امتصاص الكربون بالنسبة إلى كثافة الأشجار، والكتلة الحيوية لنبات المطاط، ومحتوى الكربون العضوي في التربة، وكذلك لرسم خرائط توزيع إمكانات الكربون باستخدام الاستشعار عن بعد. تم إجراء هذا البحث في وحدة أبحاث سنغاي بوتيه، قسم جالانغ، باستخدام طريقة المسح بجمع بيانات ثانوية وأولية. تم تحديد مواقع العينة بناءً على تصنيف مؤشر نمو النبات المعياري NDVI، بينما استُخدمت صور Landsat 9في معالجة الصور عن طريق محرك جوجل للأرض .(GEE) وجدت الدراسة أن مخزون الكربون المحتمل اختلف بين مواقع المراقبة. بناءً على الحسابات باستخدام نموذج SAVI Quadratic model (A13)، أشار توزيع الكربون، المستمد من الكتلة الحيوية الميدانية (40-80) والكربون العضوي (2-3)، إلى توزيع متوسط للكربون. كان متوسط مخزون الكربون المحتمل، المقاس من مقطع الجذع القائم، 29.43 طنًا عبر مساحة تبلغ 3.12 هكتار. سجلت الفترة 11 أعلى مخزون كربون وأكبر متوسط قطر للجذع، بمتوسط قطر 16.63 سم ومحتوى كتلة حيوية يبلغ 90.64 كجم.

الكلمات المفتاحية: الزراعة الحراجية، الهندسة البيئية، الهيفيا البرازيلية، التعلم الآلي، مؤشر الغطاء النباتي.